Cholangiocytes' Primary Cilia Regulate DNA Damage Response and Repair

Estanislao Peixoto[1,2#], Kishor Pant[1,2], Seth Richard[1], Juan E. Abrahante[3], Wioletta Czaja[4], Sergio A. Gradilone[1,2]

Affiliations:

[1]The Hormel Institute, University of Minnesota, Austin, MN 55912, USA.

[2]Masonic Cancer Center, University of Minnesota, Minneapolis, MN 55455, USA

[3]Minnesota Supercomputing Institute, University of Minnesota, Minneapolis, MN 55455, USA

[4]The University of Alabama, Birmingham, AL 35294, USA

[#]Corresponding author: Estanislao Peixoto (epeixoto@umn.edu).

Key Points

The results presented delineate the following critical observations:

i) DNA Damage Response (DDR) and DNA repair proteins localized to primary cilia structures

ii) Deciliated cells exhibited dysregulated DDR pathways, reduced survival, and S-phase arrest under genotoxic stress

iii) Elevated DNA damage was evident in deciliated cells, with increased γH2AX signals and comet assay results

iv) In vivo *IFT88* knockout mice also showed increased γH2AX expression, indicating heightened DNA damage

v) Key DDR proteins (ATM, p53, p21) were downregulated in deciliated cells after irradiation.

Abstract

Primary cilia have been considered as tumor-suppressing organelles in cholangiocarcinoma (CCA), though the mechanisms behind their protective role are not fully understood. This study investigates how the loss of primary cilia affects DNA damage response (DDR) and DNA repair processes in CCA. Human cholangiocyte cell lines were used to examine the colocalization of DNA repair proteins at the cilia and assess the impact of experimental deciliation on DNA repair pathways. Deciliation was induced using shRNA knockdown or CRISPR knockout of IFT20, IFT88, and KIF3A, followed by exposure to genotoxic agents such as cisplatin, methyl methanesulfonate (MMS), and irradiation. Cell survival, cell cycle progression, and apoptosis rates were evaluated, while DNA damage was assessed using comet assays and γH2AX

quantification. An in vivo liver-specific knockout model of *IFT88* was generated using the Cre/Lox recombination system.

Results showed that RAD51 localized at the cilia base, while ATR, PARP1, CHK1 and CHK2 were found within the cilia. Deciliated cells displayed dysregulation in critical DDR pathways. These cells also showed reduced survival and increased S-phase arrest after genotoxic challenges. Enhanced DNA damage was observed via increased γH2AX signals and comet assay results. An increase in γH2AX expression was observed in our in vivo model, indicating elevated DNA damage. Additionally, key DDR proteins, such as ATM, p53, and p21, were downregulated in deciliated cells after irradiation.

This study underscores the crucial role of primary cilia in regulating DNA repair, suggesting that targeting cilia-related mechanisms could present a novel therapeutic approach for CCA.

Keywords: cholangiocarcinoma, DNA damage response, DNA repair, genotoxins, primary cilia

Introduction

Cholangiocarcinoma (CCA), also known as bile duct cancer, represents a particularly lethal malignancy within the spectrum of liver cancers. Characterized by the malignant transformation of cholangiocytes—the epithelial cells lining the bile ducts in the liver—CCA poses significant treatment challenges due to its typically late diagnosis and limited therapeutic options (Ayala & Blackstock, 2008; Marzioni *et al.*, 2009; Banales *et al.*, 2016; Rizvi & Gores, 2017). Despite advancements in understanding liver cancers, CCA remains difficult to manage, with pharmacological treatments often showing inadequate responses and surgical intervention viable only in the early stages (Banales *et al.*, 2020). Consequently, most patients face a dismal median survival time of less than two years, underscoring the urgent need for novel therapeutic strategies (Banales *et al.*, 2020).

Primary cilia stand out as multisensory organelles ubiquitously expressed in epithelial cells, acting as cellular antennae to detect signals from the extracellular environment (Masyuk *et al.*, 2008a; Masyuk *et al.*, 2008b). We described that while cholangiocytes typically exhibit primary cilia, their expression is notably diminished in CCA cells (Gradilone *et al.*, 2013; Razumilava *et al.*, 2014; Mansini *et al.*, 2018a). The experimental removal of cilia from normal cells results in a shift towards a malignant-like behavior characterized by increased proliferation and the induction of anchorage-independent growth. Conversely, the restoration of cilia on malignant cells reverses these effects, suggesting a tumor-suppressing role for these organelles (Gradilone *et al.*, 2013). Previous results revealed the involvement of histone deacetylase 6 (HDAC6) and Sirtuin-1 in the loss of cilia within CCA cells, with its inhibition leading to the re-expression of cilia(Gradilone *et al.*, 2013; Peixoto *et al.*, 2020; Pant *et al.*, 2021). However, the

precise mechanisms through which primary cilia exert their protective influence against cancer development remain to be fully elucidated.

DNA repair processes critical for carcinogenesis suppression are intimately linked to primary cilia, especially within the centrosome at the cilia's basal body. Key DNA repair and damage response proteins, including BRCA1, BRCA2, PARP1, NBS1, ATM, ATR, CHK1, CHK2, and the pivotal cell cycle checkpoint and transcription regulator p53, are associated with this structure (Fukasawa *et al.*, 1996; Xu *et al.*, 1999; Johnson & Collis, 2016). Notably, CEP164, a centrosomal protein crucial for ciliary formation, interacts with both ATR (Ataxia Telangiectasia and Rad3-related protein) and ATM (Ataxia Telangiectasia Mutated protein). When DNA damage occurs, CEP164 undergoes phosphorylation in response, and its downregulation leads to reduced phosphorylation of other proteins in the DNA damage response, such as CHK2 and CHK1 (Sivasubramaniam *et al.*, 2008). Additionally, proteins such as MRE11, ZNF423, and CEP164, known to be linked with ciliopathies, play roles in the DNA damage response (Chaki *et al.*, 2012). Furthermore, NEK proteins participate in primary cilia function and DNA damage response (Pavan *et al.*, 2021). NEK8/NPHP9 is a ciliary kinase associated with the ciliopathies nephronophthisis and polycystic kidney disease. NEK8 suppresses double-strand breaks (DSB) by limiting cyclin A-associated CDK activity, and NEK8 mutant mice accumulate DNA damage (Choi *et al.*, 2013). Moreover, previous research has shown that disrupting ciliogenesis affects the DNA damage response, as evidenced by altered DNA-PK activity in conditions like glioblastoma (Chen *et al.*, 2021; Wei *et al.*, 2022). The presence of multiple DNA repair proteins at the ciliary basal body and the alterations observed in cells lacking cilia suggest that the loss of primary cilia in cholangiocytes might significantly affect DNA repair rates. Our work posits that the absence of primary cilia during

cholangiocarcinogenesis induces compromised DNA repair mechanisms. To explore the extent of ciliary involvement, we employed various genotoxic agents targeting different DNA repair pathways and minimized protein-specific biases using different CRISPR knockouts of key ciliary proteins.

Materials and Methods

Cell Lines and Culture

Normal human cholangiocyte (NHC) cell line was cultured in Dulbecco's Modified Eagle Medium (DMEM, Sigma-Aldrich, St. Louis, MO, USA) supplemented with 10% fetal bovine serum (FBS), 100 U/ml penicillin, 100 µg/ml streptomycin, 25 µg/ml adenine, 1 µg/ml epinephrine, 5 µg/ml insulin, 13.6 ng/ml Triiodo-L-thyronine, 8.3 µg/ml holo-transferrin, 1.3 µg/ml hydrocortisone, 10 mg/ml gentamicin, and 10 ng/ml epidermal growth factor (EGF). The HuCCT1 cell line was grown in Ham's F-12 Medium (F-12) supplemented with 10% FBS, 100 U/ml penicillin, 100 µg/ml streptomycin, and 10 mg/ml gentamicin. Cultures were maintained at 37°C in a humidified atmosphere with 5% CO2. To induce deciliation, cholangiocytes were subjected to shRNA- or CRISPR/Cas9-mediated knockdown targeting ciliary biogenesis proteins, including IFT88, IFT20, and KIF3A. Cells were exposed to irradiation using the RS 2000 Biological Research Irradiator or treated with methyl methanesulfonate (MMS, Sigma-Aldrich) or cisplatin (Tocris, Minneapolis, MN, USA).

RNA-Seq Analysis

Quality control, data alignment and gene quantification was analyzed using the CHURP pipeline(Baller *et al.*, 2019) at the University of Minnesota Supercomputing Institute (MSI). 2 x 75bp FASTQ paired-end reads for 12 samples (31.02 million reads average per sample) were

trimmed using Trimmomatic (v0.33) enabled with the optional "-q" option; 3bp sliding-window trimming from 3' end requiring minimum Q30. Quality control on raw sequence data for each sample was performed with FastQC. Read mapping was performed via HISAT2(v2.1.0) using the human genome (GRCh38.97) as reference. Gene quantification was done via Feature Counts for raw read counts. Differentially expressed genes were identified using the edgeR (negative binomial, R programming) feature in CLCGWB (Qiagen, Redwood City, CA) using raw read counts. We filtered the generated list based on a minimum 2X absolute fold change and FDR corrected $p < 0.05$. ReactomeGSA was used to analyze signaling pathways, and heatmap was generated using pheatmap (v1.0.12).

Survival and Cell Proliferation Assay

Cell proliferation was assessed using live-cell imaging assays. Specifically, 5×10^3 cells were seeded in 100 μL of culture media per well in 96-well plates. These were then incubated at 37°C and 5% CO2, utilizing the IncuCyte live-cell analysis system (Essen BioScience, Ann Arbor, MI, USA) for continuous monitoring. Data acquired was processed and analyzed using IncuCyte S3 software. To evaluate the impact of various genotoxic treatments, the proliferation rates were normalized to their corresponding untreated controls at each hourly time point assessed.

Analysis of Cell Cycle

Cells were harvested with 0.025% trypsin + 5mM EDTA in DPBS, with 2.5% FBS + 5 mM EDTA added when cells are detached. Cells were washed with cold DPBS and fixed overnight at –20°C with 70% ethanol and 30% DPBS. Fixed cells were washed with DPBS and incubated with propidium iodide, 20ug/ml and RNase A, 200 ug/ml, for 30 minutes at room temperature in the dark. Cells were analyzed on a Becton Dickinson Fortessa X-20 (BD Biosciences, San Jose,

CA, USA). Intact cells were gated in the FSC/SSC plot to exclude small debris and on a PI plot of PI-A vs. PI-W to exclude doublets. Cell cycle was determined using ModFit LT software version 5.0 (Verity Software House, Inc., Topsham, ME).

Apoptosis Assay

To assess apoptosis, cells were detached using 0.025% trypsin supplemented with 5 mM EDTA in PBS. To neutralize the trypsin, 2.5% FBS in PBS with an additional 5mM EDTA was added immediately upon cell detachment. The cell suspension was then transferred to centrifuge tubes, washed with cold PBS, and subsequently stained with Annexin V-FITC and propidium iodide (PI) for 15 minutes at room temperature in the dark. Flow cytometric analysis was performed using a Becton Dickinson Fortessa X-20 (BD Biosciences, San Jose, CA, USA). During analysis, intact cells were isolated on an FSC/SSC plot to eliminate small debris. Apoptotic cells were identified based on their staining patterns: cells in early apoptosis appeared in the lower right quadrant of the Annexin V-FITC/PI dot plot (indicating Annexin V-FITC staining only), while cells in late apoptosis or necrosis were located in the upper right quadrant (showing both Annexin V-FITC and PI staining). Data were analyzed using BD FACS DIVA software version 9.0.

Comet Assay for DNA Damage Evaluation

DNA damage was assessed using the OxiSelect Comet Assay Kit (Cell Biolabs Inc., San Diego, CA, USA), with slight modifications to the standard protocol. Normal human cholangiocyte (NHC) cells, after being treated with genotoxic agents for specified durations, were collected by double PBS washes and resuspended in 75 μL of OxiSelect Comet Agarose (prepared in PBS at pH 7.4 and maintained at 37°C). This cell-agarose mixture was promptly transferred onto glass

microscope slides pre-coated with 1% (w/v) normal melting point agarose, allowing it to solidify for 10 minutes at 4°C. Subsequently, to facilitate protein removal, the slides were submerged in lysis solution overnight at 4°C, followed by a 4-hour exposure to alkaline solution. Electrophoresis was then conducted in a buffer containing 0.3 M NaOH and 1 mM EDTA at 22 V for 35 minutes. Post-electrophoresis, slides were washed thrice with chilled distilled water (2 minutes each) and once with 70% ethanol for 5 minutes. The DNA was stained with 40 μL of Vista Green DNA Dye for visualization. The stained slides were examined under a Zeiss Axio Observer microscope equipped with Apotome, facilitating detailed analysis of the DNA damage manifested as comet tails. Comet Score (v2.0.0.0) was used to quantify the olive moment.

Immunofluorescence Assay

Cells were plated on four-well chamber slides and allowed to grow for one day. Following treatments with genotoxic agents, the cells underwent a double wash with PBS and were then fixed with ice-cold methanol for 5 minutes, followed by three washes in 0.1% PBS with Tween 20 (PBST). To block non-specific binding, cells were incubated in 3% bovine serum albumin (BSA) in PBS for 1 hour at room temperature. Subsequently, they were incubated overnight at 4°C with the following primary antibodies: anti-mouse gamma tubulin (1:200, Sigma-Aldrich), anti-rabbit or anti-mouse ARL13B (1:200, Proteintech, Rosemont, IL, USA), anti-rabbit γH2AX (1:400, Cell Signaling Technology, Danvers, MA, USA), anti-rabbit PARP1 (1:200, Proteintech), anti-rabbit RAD51 (1:200, Proteintech), anti-mouse ATR (1:200, Santa Cruz Biotechnology), anti-rabbit CHK1 (1:200, Proteintech), or anti-mouse CHK2 (1:200, Santa Cruz Biotechnology, Dallas, TX, USA). After rinsing thrice with PBST, cells were incubated with Alexa Fluor 594-conjugated goat anti-rabbit and/or Alexa Fluor 488-conjugated goat anti-mouse secondary antibodies (1:200, Life Technologies, CA, USA) for 1 hour, followed by three additional PBST

washes. Nuclei were stained with DAPI. Immunofluorescence images were acquired and analyzed using a Nikon D-eclipse C1 Si microscope or a Zeiss Axio Observer with Apotome.

Western Blot

Cells were rinsed with ice-cold PBS and lysed using RIPA buffer containing 50 mM Tris-HCl (pH 7.5), 0.1% sodium dodecyl sulfate (SDS), 0.1% Triton X-100, 1% Nonidet P-40, 0.5% sodium deoxycholate, 150 mM NaCl, and 1 mM phenylmethylsulfonyl fluoride, with the lysates incubated overnight. The lysates were then centrifuged at 13,000 rpm for 15 minutes at 4°C to pellet insoluble material. Protein concentrations were quantified using the Pierce BCA Protein Assay Kit (Thermo Scientific, Waltham, MA, USA). Proteins were separated on a 4-20% SDS-polyacrylamide gel and transferred onto nitrocellulose membranes (Bio-Rad Laboratories, Hercules, CA, USA). Membranes were blocked with 5% skim milk in TBST for 1 hour at room temperature, washed with TBST, and incubated overnight at 4°C with primary antibodies directed against anti-rabbit actin (1:1000, Sigma-Aldrich), anti-rabbit β-Actin (1:1000, Cell Signaling Technology), anti-rabbit p21 (1:1000, Cell Signaling Technology), anti-mouse p53 (1:1000, Santa Cruz Biotechnology), and anti-mouse ATM (1:1000, Santa Cruz Biotechnology). Following three TBST washes, membranes were incubated with HRP-conjugated secondary antibodies in 5% skim milk in TBST for 1 hour at room temperature. Detection was performed using the Pierce ECL Western Blotting Substrate (Thermo Scientific, Rockford, IL, USA).

Animal studies

Alb-Cre-IFT88KO mice on a C57BL/6J background were housed in a dedicated animal facility under a 12-hour light-dark cycle with ad libitum access to a standard diet and water. Liver samples were obtained from 48-week-old mice. All animal procedures were conducted in

accordance with protocols approved by the University of Minnesota Institutional Animal Care and Use Committee (IACUC).

Statistical analysis

Data are presented as mean ± standard error (SE). Statistical comparisons were conducted using one- or two-way ANOVA, Student's unpaired t-test or the Mann-Whitney U test, as appropriate. Significance levels were set at $P < 0.05$, $P < 0.01$, $P < 0.001$, and $P < 0.0001$. Experiments were conducted at least twice when using different clones of the same mutation, as well as different CRISPR mutations targeted for ciliary loss. If only a single clone was used, experiments were performed independently at least three times.

Results

DNA Damage Response Proteins colocalize with ciliary structures.

Our investigation began by examining whether DNA damage response (DDR) proteins and DNA repair proteins colocalize at the base of primary cilia in cholangiocytes. Utilizing immunofluorescence assays on normal human cholangiocyte (NHC) cells, we observed that RAD51 localize at the base of the cilia. Additionally, ATR, PARP1, CHK1 and CHK2 exhibited colocalization within the ciliary structure (Figure 1A). This suggests a spatial association between these DDR proteins and the primary cilium, hinting at a potential functional interplay in DNA repair processes.

To further explore the relationship between DDR mechanisms and primary cilia, we conducted RNA sequencing analysis on NHC cells with shIFT88-mediated deciliation. The analysis, performed using Reactome Gene Set Analysis (GSA), revealed a downregulation in the expression of genes associated with DNA Damage Response Pathways, Base Excision Repair,

DNA Damage Reversal, and DNA Double-Strand Break Repair pathways in deciliated NHC cells (Table I). We generated a heatmap using the most relevant genes involved in DNA repair and the DNA damage response. The analysis revealed a predominant downregulation of these genes in deciliated cells (Figure 1B). These findings underscore the impact of cilia loss on the cellular capacity to manage and repair DNA damage, emphasizing the integral role of primary cilia in maintaining genomic integrity.

Primary cilia loss impairs Cholangiocytes Survival Under Genotoxic Stress.

We explored the effects of deciliation on the survival of cholangiocytes when exposed to genotoxic agents, given the established link between decreased DNA repair pathway activity and perturbed proliferation. To target different types of DNA damage, we employed various genotoxic approaches, including irradiation to induce primarily double-strand breaks, methyl methanesulfonate (MMS) to cause single-strand breaks, and cisplatin to induce DNA crosslinking. Using live cell imaging, we assessed the proliferation of normal human cholangiocyte (NHC) cells subjected to genotoxic challenges. Our findings revealed a significant reduction in the survival of mostly of the deciliated NHC cells following exposure to 5 Gy of irradiation, 48-hour treatment with 2.5 µM cisplatin, or treatment with 1 mM methyl methanesulfonate, in comparison to their control ciliated counterparts (Figure 2A). Interestingly, tumoral cells, such as HuCCT1, which do not express cilia can recover ciliary expression by treating them with an HDAC6 inhibitor like ACY1215 (Peixoto *et al.*, 2020). Upon challenging these ciliogenesis-induced HuCCT1 cells with MMS, an increase in survival was observed compared to control tumor cells (Figure 2B). Taken together, these data suggest that the presence of primary cilia enhances cellular resilience against genotoxic stress, highlighting the protective role of primary cilia in maintaining genomic integrity.

To elucidate the impact of cilia loss on cell survival mechanisms, we analyzed the cell cycle distribution and apoptosis rates in challenged cells. Our findings indicate that MMS challenged cells lacking cilia demonstrate increased arrest in the S phase (Figure 3A). This may suggest that stalled replication due to DNA damage actively prevents progression through the cell cycle in the absence of primary cilia. For irradiated deciliated cells, we observed a slight trend increase in S phase, except in KIF3A mutants. In response to cisplatin treatment, we noted a slight trend decrease in G2 phase arrest in deciliated cells, except in IFT88-deficient cells. Furthermore, compared to their ciliated counterparts, deciliated irradiated cells exhibited a slight increase in apoptosis rates (Figure 3B). This slightly elevation in apoptosis suggests that the inability of deciliated cells to effectively repair DNA damage may contribute to their increased susceptibility to programmed cell death, even if the difference is not statistically significant.

Increased DNA Damage in Deciliated Cholangiocytes.

Phosphorylated H2AX (γH2AX) plays a crucial role in anchoring DNA repair machinery at sites of DNA damage, while its absence can lead to genomic instability and cancer progression (Scully & Xie, 2013). In our study, we observed elevated γH2AX levels in deciliated normal human cholangiocyte (NHC) cells exposed to 5 Gy of radiation at both 30 minutes and 6 hours post-exposure. Furthermore, RAD51, essential for homologous recombination (HR) repair of DSBs, showed increased levels in deciliated NHC cells 6 and 24 hours after 5 Gy radiation exposure compared to irradiated controls, hinting at RAD51 activity dysregulation (Figure 4A). Additionally, deciliated NHC cells treated with 2.5 mM cisplatin for 24 hours or with MMS for 1 hour, followed by a 24-hour recovery, exhibited higher γH2AX levels compared to ciliated controls. (Figure 4B, C). Taken together, these results suggest either enhanced γH2AX activity or impaired resolution of double-strand breaks (DSBs) in deciliated cells. Since our *in vitro* studies

indicated increased DNA damage in cells lacking primary cilia, we investigated whether a similar effect occurs *in vivo* using IFT88 knockout mice to support the hypothesis that the absence of primary cilia impairs DNA repair. As expected, IFT88 knockout mice display a significant reduction in primary cilia expression (Pant *et al.*, 2024). These 48-week-old animals displayed elevated levels of γH2AX compared to controls (Figure 4D), suggesting that the absence of primary cilia may render cells more susceptible to physiological stress.

To further quantify DNA damage, we employed a comet assay using cells challenged with methyl methanesulfonate (MMS) or irradiation as genotoxic agents. Since the formation of crosslinks affects the migration of DNA fragments, we did not include cisplatin in these experiments. Mostly of the deciliated cells exhibited significantly more DNA damage 24 hours after following 1 hour of treatment with 1 mM MMS or after exposure to 10 Gy of irradiation, in contrast to cells with intact cilia while a minority of the clones showed not change (Figure 5A, B).

Dysregulation of DNA Damage Response Proteins in Deciliated Cells.

To explore the impact of primary cilia loss on the DNA damage response, we conducted an analysis of CRISPR IFT88-deciliated cells following exposure to 5 Gy of irradiation. In normal ciliated cells, irradiation induces DNA double-strand breaks, leading to the rapid activation of the ATM kinase. ATM phosphorylates and stabilizes p53, a key tumor suppressor, which then drives the expression of downstream targets such as p21. The activation of this pathway in response to DNA damage is crucial for maintaining genomic stability, as it prevents cells with damaged DNA from progressing through the cell cycle. By studying deciliated IFT88 cells, we aimed to determine whether the absence of primary cilia disrupts this ATM-p53-p21 axis and compromises the cell's ability to manage DNA damage, potentially leading to impaired repair

mechanisms or altered cell fate decisions, such as increased apoptosis or genomic instability. Our findings indicate dysregulation of key DNA damage response proteins in deciliated cells. Specifically, deciliated NHC cells exhibit a reduction in ATM levels 24 hours post-5 Gy irradiation (Figure 6A, B). Additionally, NHC deciliated cells show a decrease in p53 levels at 6 hours following 5 Gy irradiation (Figure 6C). Moreover, we observed an increase in p21 levels in NHC cells 24 hours after irradiation (Figure 6D) but the increase was lower on deciliated cells.

Discussion

Previous work has suggested that the lack or impairment of primary cilia, as well as disturbances in the signaling pathways linked to cilia, could facilitate oncogenic processes in cholangiocytes (Gradilone *et al.*, 2013; Mansini *et al.*, 2018b; Peixoto *et al.*, 2020; Pant *et al.*, 2021). The results presented here delineate the following critical observations: i) DDR proteins, including Rad51, ATR, PARP1, CHK1, and CHK2 co-localize with ciliary structures within cholangiocytes; ii) the absence of cilia in cholangiocytes leads to an aberrant expression profile of DDR mRNA; iii) cholangiocytes that are devoid of cilia demonstrate an increased sensitivity towards genotoxic agents; iv) such deciliated cells manifest an elevated level of γH2AX in response to genotoxic stress, while a liver specific *IFT88* knockout mouse model shows elevated levels of γH2AX in the ciliary defective cholangiocytes; v) an enhanced accumulation of DNA damage is observed in deciliated cells; and vi) upon exposure to genotoxic stimuli, there is a noticeable reduction in the presence of DDR proteins in deciliated cells. Collectively, these findings underscore, for the first time, the critical role of cilia in maintaining genomic stability in cholangiocytes. We observed the impact of ciliary loss on DNA repair across three distinct DNA damage models, including alkylations (MMS), double-strand breaks (irradiation), and DNA crosslinks (cisplatin). These results reinforce the idea that primary cilia play a conserved role in orchestrating the DNA

damage response. Furthermore, the results were consistently replicated across different genetic approaches to deciliation using CRISPR knockouts of IFT88, KIF3A, or IFT20, indicating that the process is cilia-dependent rather than protein-specific.

PARP was observed to co-localize with centrosomes in mouse embryonic fibroblasts, human osteogenic sarcoma, and human glioma cells (Kanai *et al.*, 2000; Kanai *et al.*, 2003). Similarly, ATM, ATR, CHK1, and CHK2 showed co-localization with centrosomes in HeLa cells (Zhang *et al.*, 2007). Our investigations into cholangiocytes revealed a comparable co-localization pattern during interphase, with the proteins ATM, PARP1, CHK1 and CHK2 also present on the cilia. This suggests that the microtubules organized by the centrosomes may serve as a conduit for the trafficking of DNA repair proteins, potentially influenced by ciliary signaling mechanisms. Notably, the efficacy of DNA-damaging agents is augmented by microtubule targeting agents, which disrupt the trafficking pathway of DNA repair proteins (Poruchynsky *et al.*, 2015).

Our findings demonstrate that the absence of primary cilia increases sensitivity to DNA damage in cholangiocytes, as evidenced by the use of various genotoxins and deciliation approaches and assessed through γH2AX and comet assays. Additionally, our in vivo results show that under basal conditions, the knockout (KO) of IFT88 increases γH2AX foci. Our results align with and build upon previous findings from different models. Other authors have showed that the knockout of IFT88 and CEP164 attenuates the DNA damage response via diminished DNA-PK-p53 activation in human retinal pigment epithelial (RPE1) cells (Chen *et al.*, 2021). Additionally, primary cilia have been implicated in meiotic recombination and the repair of double strand breaks during gametogenesis in zebrafish (Xie *et al.*, 2022). Moreover, the inhibition of ciliogenesis has been shown to augment sensitivity to Temozolomide and ionizing radiation in human glioblastoma cells (Wei *et al.*, 2022), while the loss of primary cilia is correlated with

genomic instability in medulloblastoma (Youn *et al.*, 2022). Kidney tubular cells exhibiting reduced ciliary length demonstrated an increased sensitivity to apoptosis induced by cisplatin, as evidenced in previous studies (Wang *et al.*, 2013). Similarly, the deficiency of IFT88 in proximal tubular cells, explored through an in vivo knockout (KO) murine model, also resulted in heightened sensitivity to cisplatin (Wang *et al.*, 2021). Collectively, these observations underscore the pivotal role of primary cilia in the maintenance of genomic integrity and in modulating the cellular response to DNA damage across various cell types and conditions.

The fact that deciliated cells have decreased levels of p53 and p21 and increased levels of γH2AX and Rad51 indicates that their DNA damage response and repair mechanisms are deregulated; however, the ciliary-dependent mechanisms regulating these processes remain unknown. A ciliary pathway that may be implicated in our observations would be related to Liver kinase B1 (LKB1). Found in both ciliary and cytoplasmic locations, LKB1 plays a role in the DNA damage response by phosphorylating various downstream proteins. Its deficiency leads to delayed DNA damage repair (Wang *et al.*, 2016). Treatment with ATP, which activates LKB1, induces an increase in p-PTEN and inhibits AKT, but only in ciliated cells (Mansini *et al.*, 2018b). PTEN, in turn, regulates p53 expression and activity through phosphatase-dependent and expression mechanisms, and also contributes significantly to DNA damage repair and response (Freeman *et al.*, 2003). For example, upregulation of PTEN inhibits AKT and MDM2, which also increase levels of p53 (Ming & He, 2012). Other ciliary pathways may be also related to cilia and the DNA damage response, in particular Wnt and Hedgehog (Shen *et al.*, 2019). B-catenin by Wnt is indirectly involved in activation of p53 and expression of H2AX (Karimaian *et al.*, 2017). Hedgehog signaling GLI proteins can interfere with almost all DNA repair types (Meng *et al.*, 2015).

The fact that primary cilia have a role in DNA repair is particularly important in CCA, because cholangiocytes are among the cells more exposed to genotoxins generated as hepatic metabolic end products (Chaki *et al.*, 2012). In summary, the intricate relationship between primary cilia and DNA repair proteins indicates that the absence of primary cilia in tumor cells could potentially alter the efficiency of DNA repair processes. Understanding the mechanisms that link the primary cilium with its tumor suppressor characteristics may lead to new therapies for CCA, which currently has dismal prognosis with no effective therapies.

Funding

This work was supported by The Hormel Foundation, National Institutes of Health Grant R01DK132781 (to S.A.G.) and NIH grant R01-GM-143428 (to W.C.). The content is solely the responsibility of the authors and does not necessarily represent the official views of The Hormel Foundation or the National Institutes of Health.

Acknowledgments

We would like to thank Tanner Conway and Todd Schuster for expert technical assistance.

Figures

Figure 1. DNA damage response genes colocalize with the base of the cilia and the deciliation process impacts DDR and DNA repair pathways. (A) Immunofluorescences for RAD51, ATR, CHK1, CHK2 and PARP1 of NHC cells (630X, inset shows an amplification of the ciliary

structures, highlighted by the yellow arrow). (B) Heatmap analysis comparing the gene expression of NHC shNT cells and shIFT88 cells.

Figure 2. Deciliated cholangiocytes show lower survival than normal cholangiocytes when challenged by genotoxics. (A) Survival curves of NHC cilated and deciliated cells treated with 1 mM MMS, 2.5 µM cisplatin or 5Gy relative to their respective controls (One Way Anova, *p<0.05, **p<0.01, ***p<0.001, ****p<0.0001). (B) Survival curves of CCA cells treated or not with ACY1215 and/or MMS (One Way Anova, **p<0.01).

Figure 3. Apoptosis and cell cycle dynamics of ciliated and deciliated cells in response to genotoxic treatments. (A) Stacked bar graphs representing the percentage of cells in each step of the cell cycle of ciliated and deciliated cells on basal conditions or 24 hs after 2.5 µM cisplatin, 1 mM MMS or 5 Gy (One-way ANOVA, **p<0.01, for the S phase comparison between NT #4 MMS-treated cells and MMS-treated deciliated clones). (B) Stacked bar graphs representing the percentage of cells in apoptosis, late apoptosis/early necrosis, and necrosis of ciliated and deciliated cells on basal conditions or 24 hs after 2.5 µM cisplatin, 1 mM MMS or 5 Gy.

Figure 4. γH2AX is increased on deciliated cells after genotoxics. (A) Immunofluorescence for γH2AX of NHC ciliated and deciliated cells at 30 min, 6h and 24 hs after 5 Gy irradiation (One Way Anova, ****p<0.0001, 630X). (B) Immunofluorescence for γH2AX of NHC ciliated and deciliated cells at 24 hs after treatment with 2.5 µM cisplatin (One Way Anova, ****p<0.0001, 630X). (C) Immunofluorescence for γH2AX of NHC ciliated and deciliated cells at 24 hs after treatment with 1 mM MMS (One Way Anova, ****p<0.0001, 630X). (D) Immunofluorescence staining and quantification of γH2AX in IFT88 knockout mice (n=3, unpaired t-test, ****p<0.0001, magnification x630). The inset shows the IFT88/LOX construct, illustrating the Albumin-Cre–mediated conditional knockout design.

Figure 5. DNA damage is increased on deciliated cells after genotoxics. Representative pictures and quantification of a Comet Assay of ciliated and deciliated (clones KIF3A #1, KIF3A #2, KIF3A #17, IFT20 #33, IFT88 #13 and IFT88 #19) NHC cells after 4h or 24h of a treatment with 10 Gy irradiation (A) or 1 mM MMS (B) (One Way Anova, ***p<0.001, ****p<0.0001, 100X).

Figure 6. DNA damage response proteins are dysregulated on deciliated cells after irradiation. (A) Western blot analysis of control and IFT88-deficient cells following 5 Gy irradiation, using antibodies against ATM, p53, p21, and actin. (B) ATM Western blot analysis of NHC ciliated and deciliated cells treated with 5 Gy (2-way Anova, **p<0.01, ***p<0.001). (C) p53 Western blot analysis of NHC ciliated and deciliated cells treated with 5 Gy (2-way Anova, *p<0.05, **p<0.01). (D) p21 Western blot analysis of NHC ciliated and deciliated cells treated with 5 Gy (2-way Anova, *p<0.05, **p<0.01).

Table I

Table I. DNA repair and DNA damage response pathways affected by the loss of primary cilia (IFT88 KO)

ame	Direction	FDR	Pvalue	Ngenes	FoldChange
53-Independent DNA Damage esponse	Down	0.000725476	1.27242E-05	48	-0.399972034
53-Independent G1/S DNA damage heckpoint	Down	0.000725476	1.27242E-05	48	-0.399972034
2/M Checkpoints	Down	0.003245501	9.36819E-05	140	-0.328135695
tabilization of p53	Down	0.003448947	0.000100918	53	-0.335851291
ell Cycle Checkpoints	Down	0.004040795	0.000121432	263	-0.254885353
1/S DNA Damage Checkpoints	Down	0.011158314	0.000436802	64	-0.242443097
53-Dependent G1 DNA Damage esponse	Down	0.014526662	0.000603124	62	-0.236900968
53-Dependent G1/S DNA damage heckpoint	Down	0.014526662	0.000603124	62	-0.236900968
NA Double-Strand Break Repair	Down	0.287105617	0.027691125	141	-0.252241701
ase Excision Repair	Down	0.310922161	0.032088052	63	-0.307230762
GMT-mediated DNA damage reversal	Down	0.311882094	0.032685117	1	-7.773664412
omology Directed Repair	Down	0.320358055	0.034455275	112	-0.219061061
epurination	Down	0.345700492	0.042713555	28	-0.543145169
leavage of the damaged purine	Down	0.345700492	0.042713555	28	-0.543145169

ensing of DNA Double Strand Breaks	Down	0.360328534	0.049825588	6	-0.41684425

Declaration of generative AI and AI-assisted technologies in the writing process

During the preparation of this work the author(s) used ChatGPT to check and correct the English language. After using this tool/service, the author(s) reviewed and edited the content as needed and take(s) full responsibility for the content of the publication.

Bibliography

Ayala D & Blackstock AW. (2008). Effective treatment strategies for cholangiocarcinoma: the challenge remains. *Gastrointestinal cancer research : GCR* **2,** 251-252.

Baller J, Kono T, Herman A & Zhang Y. (2019). CHURP: A Lightweight CLI Framework to Enable Novice Users to Analyze Sequencing Datasets in Parallel. *Pearc '19: Proceedings of the Practice and Experience in Advanced Research Computing on Rise of the Machines (Learning)*.

Banales JM, Cardinale V, Carpino G, Marzioni M, Andersen JB, Invernizzi P, Lind GE, Folseraas T, Forbes SJ, Fouassier L, Geier A, Calvisi DF, Mertens JC, Trauner M, Benedetti A, Maroni L, Vaquero J, Macias RI, Raggi C, Perugorria MJ, Gaudio E, Boberg KM, Marin JJ & Alvaro D. (2016). Expert consensus document: Cholangiocarcinoma: current knowledge and future perspectives consensus statement from the European Network for the Study of Cholangiocarcinoma (ENS-CCA). *Nat Rev Gastroenterol Hepatol* **13,** 261-280.

Banales JM, Marin JJG, Lamarca A, Rodrigues PM, Khan SA, Roberts LR, Cardinale V, Carpino G, Andersen JB, Braconi C, Calvisi DF, Perugorria MJ, Fabris L, Boulter L, Macias RIR, Gaudio E, Alvaro D, Gradilone SA, Strazzabosco M, Marzioni M, Coulouarn C, Fouassier L, Raggi C, Invernizzi P, Mertens JC, Moncsek A, Rizvi S, Heimbach J, Koerkamp BG, Bruix J, Forner A, Bridgewater J, Valle JW & Gores GJ. (2020). Cholangiocarcinoma 2020: the next horizon in mechanisms and management. *Nat Rev Gastroenterol Hepatol* **17,** 557-588.

Chaki M, Airik R, Ghosh AK, Giles RH, Chen R, Slaats GG, Wang H, Hurd TW, Zhou W, Cluckey A, Gee HY, Ramaswami G, Hong CJ, Hamilton BA, Cervenka I, Ganji RS, Bryja V, Arts HH, van Reeuwijk J, Oud MM, Letteboer SJ, Roepman R, Husson H, Ibraghimov-Beskrovnaya O, Yasunaga T, Walz G, Eley L, Sayer JA, Schermer B, Liebau MC, Benzing T, Le Corre S, Drummond I, Janssen S, Allen SJ, Natarajan S, O'Toole JF, Attanasio M, Saunier S, Antignac C, Koenekoop RK, Ren H, Lopez I, Nayir A, Stoetzel C, Dollfus H, Massoudi R, Gleeson JG, Andreoli SP, Doherty DG, Lindstrad A, Golzio C, Katsanis N, Pape L, Abboud EB, Al-Rajhi AA, Lewis RA, Omran H, Lee EY, Wang S, Sekiguchi JM, Saunders R, Johnson CA, Garner E, Vanselow K, Andersen JS, Shlomai J, Nurnberg G, Nurnberg P, Levy S, Smogorzewska A, Otto EA & Hildebrandt F. (2012). Exome capture reveals ZNF423 and CEP164 mutations, linking renal ciliopathies to DNA damage response signaling. *Cell* **150,** 533-548.

Chen TY, Huang BM, Tang TK, Chao YY, Xiao XY, Lee PR, Yang LY & Wang CY. (2021). Genotoxic stress-activated DNA-PK-p53 cascade and autophagy cooperatively induce ciliogenesis to maintain the DNA damage response. *Cell Death Differ* **28,** 1865-1879.

Choi HJ, Lin JR, Vannier JB, Slaats GG, Kile AC, Paulsen RD, Manning DK, Beier DR, Giles RH, Boulton SJ & Cimprich KA. (2013). NEK8 links the ATR-regulated replication stress response and S phase CDK activity to renal ciliopathies. *Mol Cell* **51,** 423-439.

467 Freeman DJ, Li AG, Wei G, Li HH, Kertesz N, Lesche R, Whale AD, Martinez-Diaz H, Rozengurt N, Cardiff
468 RD, Liu X & Wu H. (2003). PTEN tumor suppressor regulates p53 protein levels and activity
469 through phosphatase-dependent and -independent mechanisms. *Cancer Cell* **3,** 117-130.

470

471 Fukasawa K, Choi T, Kuriyama R, Rulong S & Vande Woude GF. (1996). Abnormal centrosome
472 amplification in the absence of p53. *Science* **271,** 1744-1747.

473

474 Gradilone SA, Radtke BN, Bogert PS, Huang BQ, Gajdos GB & LaRusso NF. (2013). HDAC6 inhibition
475 restores ciliary expression and decreases tumor growth. *Cancer Res* **73,** 2259-2270.

476

477 Johnson CA & Collis SJ. (2016). Ciliogenesis and the DNA damage response: a stressful relationship. *Cilia*
478 **5**.

479

480 Kanai M, Tong WM, Sugihara E, Wang ZQ, Fukasawa K & Miwa M. (2003). Involvement of poly(ADP-
481 Ribose) polymerase 1 and poly(ADP-Ribosyl)ation in regulation of centrosome function. *Mol Cell*
482 *Biol* **23,** 2451-2462.

483

484 Kanai M, Uchida M, Hanai S, Uematsu N, Uchida K & Miwa M. (2000). Poly(ADP-ribose) polymerase
485 localizes to the centrosomes and chromosomes. *Biochem Biophys Res Commun* **278,** 385-389.

486

487 Karimaian A, Majidinia M, Baghi HB & Yousefi B. (2017). The crosstalk between Wnt/beta-catenin
488 signaling pathway with DNA damage response and oxidative stress: Implications in cancer
489 therapy. *DNA Repair* **51,** 14-19.

490

491 Mansini AP, Lorenzo Pisarello MJ, Thelen KM, Cruz-Reyes M, Peixoto E, Jin S, Howard BN, Trussoni CE,
492 Gajdos GB, LaRusso NF, Perugorria MJ, Banales JM & Gradilone SA. (2018a). MiR-433 and miR-22
493 dysregulations induce HDAC6 overexpression and ciliary loss in cholangiocarcinoma. *Hepatology***,**
494 561-573.

495

496 Mansini AP, Peixoto E, Jin S, Richard S & Gradilone SA. (2018b). The chemosensory function of primary
497 cilia regulates cholangiocyte migration, invasion and tumor growth. *Hepatology***,** 1582-1598.

498

499 Marzioni M, Invernizzi P, Candelaresi C, Maggioni M, Saccomanno S, Selmi C, Rychlicki C, Agostinelli L,
500 Cassani B, Miozzo M, Pasini S, Fava G, Alpini G & Benedetti A. (2009). Human
501 cholangiocarcinoma development is associated with dysregulation of opioidergic modulation of
502 cholangiocyte growth. *Digestive and liver disease : official journal of the Italian Society of*
503 *Gastroenterology and the Italian Association for the Study of the Liver* **41,** 523-533.

504

505 Masyuk AI, Gradilone SA, Banales JM, Huang BQ, Masyuk TV, Lee SO, Splinter PL, Stroope AJ & LaRusso
506 NF. (2008a). Cholangiocyte primary cilia are chemosensory organelles that detect biliary
507 nucleotides via P2Y12 purinergic receptors. *Am J Physiol Gastrointest Liver Physiol* **295,** G725-
508 G734.

509
510 Masyuk AI, Masyuk TV & LaRusso NF. (2008b). Cholangiocyte primary cilia in liver health and disease.
511 *Dev Dyn* **237,** 2007-2012.

512
513 Meng E, Hanna A, Samant RS & Shevde LA. (2015). The Impact of Hedgehog Signaling Pathway on DNA
514 Repair Mechanisms in Human Cancer. *Cancers (Basel)* **7,** 1333-1348.

515
516 Ming M & He YY. (2012). PTEN in DNA damage repair. *Cancer Lett* **319,** 125-129.

517
518 Pant K, Peixoto E, Richard S, Biswas A, O'Sullivan MG, Giama N, Ha Y, Yin J, Carotenuto P, Salati M, Ren Y,
519 Yang R, Franco B, Roberts LR & Gradilone SA. (2021). Histone Deacetylase Sirtuin 1 Promotes
520 Loss of Primary Cilia in Cholangiocarcinoma. *Hepatology* **74,** 3235-3248.

521
522 Pant K, Richard S, Peixoto E, Baral S, Yang R, Ren Y, Masyuk TV, LaRusso NF & Gradilone SA. (2024).
523 Cholangiocyte ciliary defects induce sustained epidermal growth factor receptor signaling.
524 *Hepatology*.

525
526 Pavan ICB, de Oliveira AP, Dias PRF, Basei FL, Issayama LK, Ferezin CD, Silva FR, de Oliveira ALR, Moura
527 LAD, Martins MB, Simabuco FM & Kobarg J. (2021). On Broken Ne(c)ks and Broken DNA: The
528 Role of Human NEKs in the DNA Damage Response. *Cells* **10**.

529
530 Peixoto E, Jin S, Thelen K, Biswas A, Richard S, Morleo M, Mansini A, Holtorf S, Carbone F, Pastore N,
531 Ballabio A, Franco B & Gradilone SA. (2020). HDAC6-dependent ciliophagy is involved in ciliary
532 loss and cholangiocarcinoma growth in human cells and murine models. *Am J Physiol*
533 *Gastrointest Liver Physiol* **318,** G1022-G1033.

534
535 Poruchynsky MS, Komlodi-Pasztor E, Trostel S, Wilkerson J, Regairaz M, Pommier Y, Zhang X, Kumar Maity
536 T, Robey R, Burotto M, Sackett D, Guha U & Fojo AT. (2015). Microtubule-targeting agents
537 augment the toxicity of DNA-damaging agents by disrupting intracellular trafficking of DNA
538 repair proteins. *Proc Natl Acad Sci U S A* **112,** 1571-1576.

539
540 Razumilava N, Gradilone SA, Smoot RL, Mertens JC, Bronk SF, Sirica AE & Gores GJ. (2014). Non-canonical
541 Hedgehog signaling contributes to chemotaxis in cholangiocarcinoma. *Journal of hepatology* **60,**
542 599-605.

543
544 Rizvi S & Gores GJ. (2017). Emerging molecular therapeutic targets for cholangiocarcinoma. *J Hepatol*.

545
546 Scully R & Xie A. (2013). Double strand break repair functions of histone H2AX. *Mutat Res* **750,** 5-14.

547

Shen T, Gao K, Hu Z, Miao Y & Wang X. (2019). Ciliary Mechanism of Regulating Hedgehog and Wnt/beta-Catenin Signaling Modulates Ultraviolet B Irradiation-Induced Photodamage in HaCaT Cells. *J Biomed Nanotechnol* **15,** 196-203.

Sivasubramaniam S, Sun XM, Pan YR, Wang SH & Lee EYHP. (2008). Cep164 is a mediator protein required for the maintenance of genomic stability through modulation of MDC1, RPA, and CHK1. *Gene Dev* **22,** 587-600.

Wang S, Wei Q, Dong G & Dong Z. (2013). ERK-mediated suppression of cilia in cisplatin-induced tubular cell apoptosis and acute kidney injury. *Biochim Biophys Acta* **1832,** 1582-1590.

Wang S, Zhuang S & Dong Z. (2021). IFT88 deficiency in proximal tubular cells exaggerates cisplatin-induced injury by suppressing autophagy. *Am J Physiol Renal Physiol* **321,** F269-F277.

Wang YS, Chen J, Cui F, Wang H, Wang S, Hang W, Zeng Q, Quan CS, Zhai YX, Wang JW, Shen XF, Jian YP, Zhao RX, Werle KD, Cui R, Liang J, Li YL & Xu ZX. (2016). LKB1 is a DNA damage response protein that regulates cellular sensitivity to PARP inhibitors. *Oncotarget* **7,** 73389-73401.

Wei L, Ma W, Cai H, Peng SP, Tian HB, Wang JF, Gao L & He JP. (2022). Inhibition of Ciliogenesis Enhances the Cellular Sensitivity to Temozolomide and Ionizing Radiation in Human Glioblastoma Cells. *Biomed Environ Sci* **35,** 419-436.

Xie H, Wang X, Jin M, Li L, Zhu J, Kang Y, Chen Z, Sun Y & Zhao C. (2022). Cilia regulate meiotic recombination in zebrafish. *J Mol Cell Biol* **14**.

Xu X, Weaver Z, Linke SP, Li C, Gotay J, Wang XW, Harris CC, Ried T & Deng CX. (1999). Centrosome amplification and a defective G2-M cell cycle checkpoint induce genetic instability in BRCA1 exon 11 isoform-deficient cells. *Mol Cell* **3,** 389-395.

Youn YH, Hou S, Wu CC, Kawauchi D, Orr BA, Robinson GW, Finkelstein D, Taketo MM, Gilbertson RJ, Roussel MF & Han YG. (2022). Primary cilia control translation and the cell cycle in medulloblastoma. *Genes Dev* **36,** 737-751.

Zhang S, Hemmerich P & Grosse F. (2007). Centrosomal localization of DNA damage checkpoint proteins. *J Cell Biochem* **101,** 451-465.

Competing Interests

No conflicts of interests

586

A

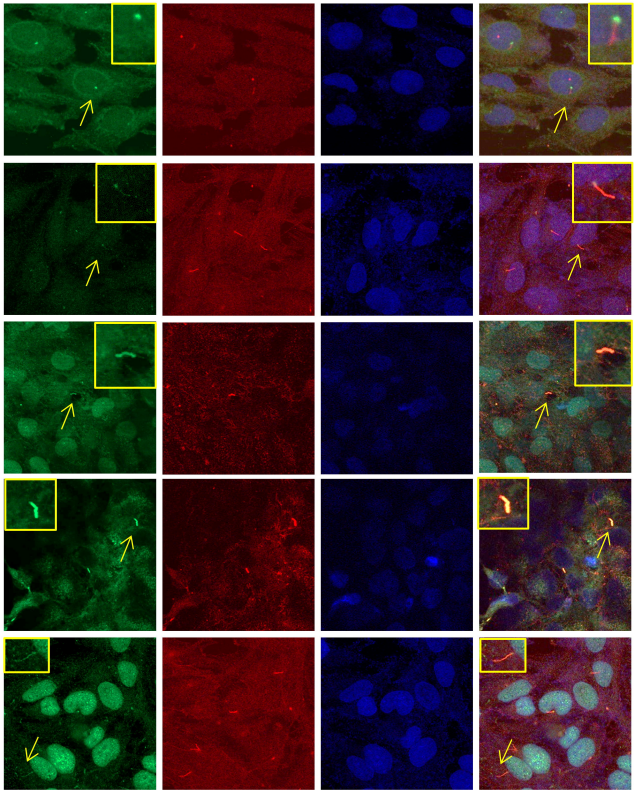
Rad51
ARL13B
DAPI
ATR
ARL13B
DAPI
PARP1
ARL13B
DAPI
CHK1
ARL13B
DAPI
CHK2
ARL13B
DAPI

B

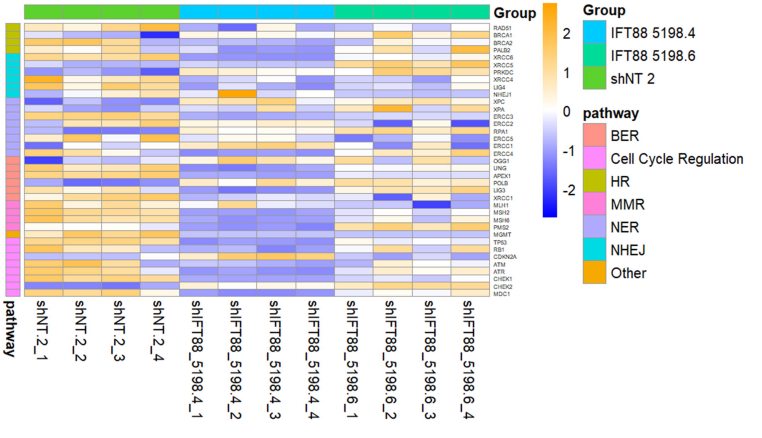
Group
pathway
shNT.2_1
shNT.2_2
shNT.2_3
shNT.2_4
shIFT88_5198.4_1
shIFT88_5198.4_2
shIFT88_5198.4_3
shIFT88_5198.4_4
shIFT88_5198.6_1
shIFT88_5198.6_2
shIFT88_5198.6_3
shIFT88_5198.6_4
2
1
0
-1
-2
Group
IFT88 5198.4
IFT88 5198.6
shNT 2
pathway
BER
Cell Cycle Regulation
HR
MMR
NER
NHEJ
Other

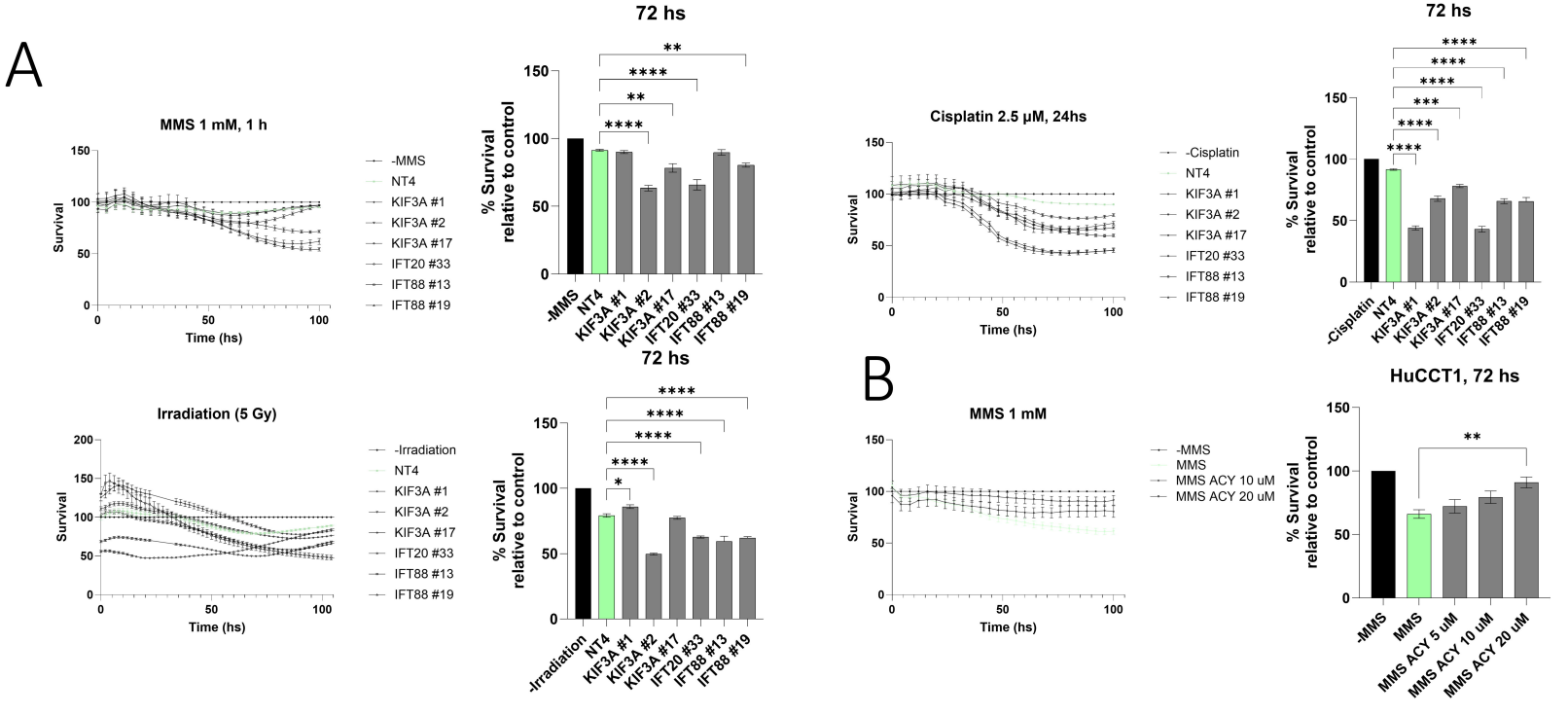
A
MMS 1 mM, 1 h
Survival
Time (hs)
-MMS
NT4
KIF3A #1
KIF3A #2
KIF3A #17
IFT20 #33
IFT88 #13
IFT88 #19
72 hs
% Survival relative to control
Cisplatin 2.5 µM, 24hs
-Cisplatin
Irradiation (5 Gy)
-Irradiation
B
MMS 1 mM
MMS
MMS ACY 10 uM
MMS ACY 20 uM
HuCCT1, 72 hs
MMS ACY 5 uM

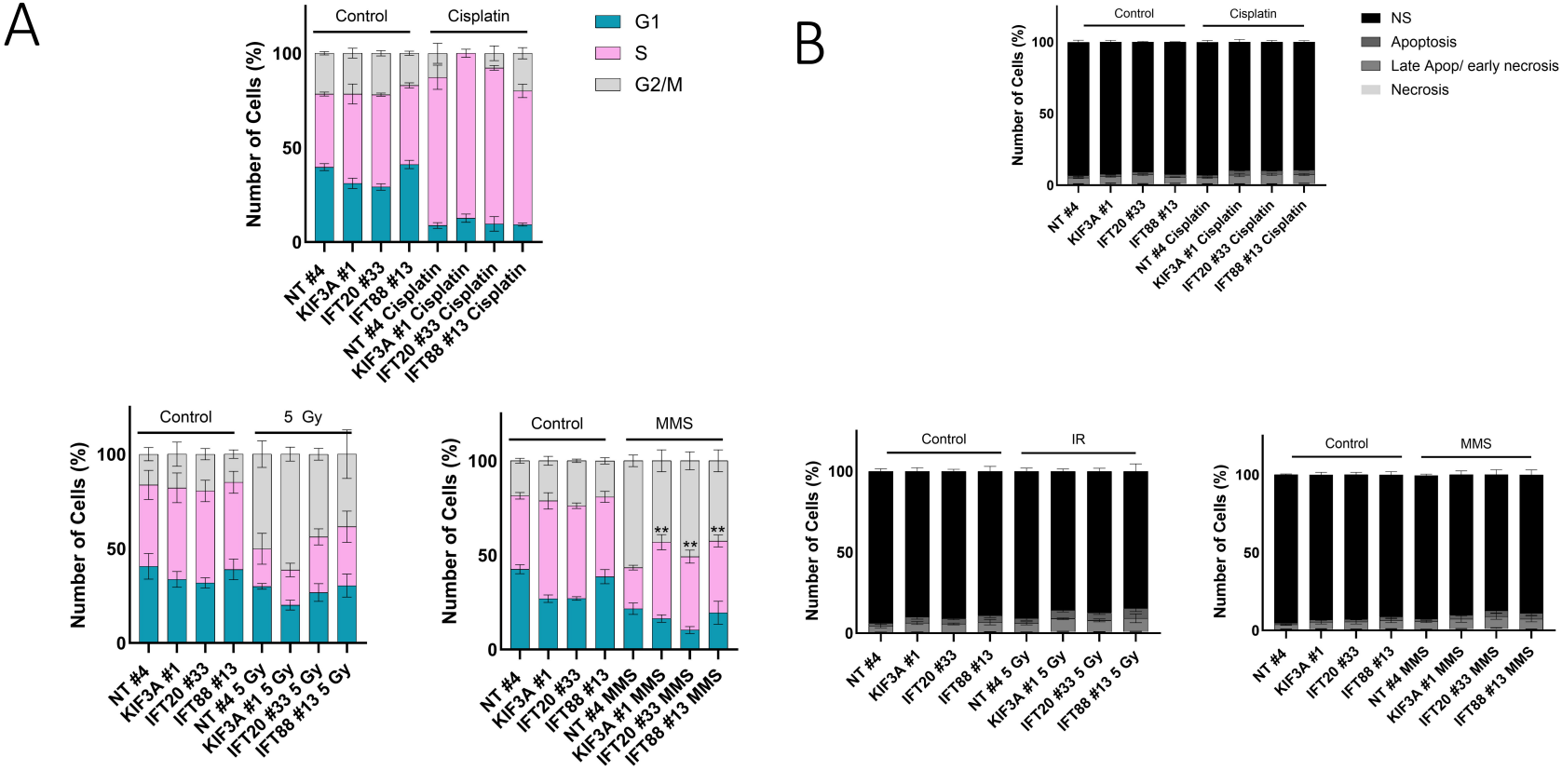
A
Control
Cisplatin
G1
S
G2/M
Number of Cells (%)
100
50
0
NT #4
KIF3A #1
IFT20 #33
IFT88 #13
NT #4 Cisplatin
KIF3A #1 Cisplatin
IFT20 #33 Cisplatin
IFT88 #13 Cisplatin
B
NS
Apoptosis
Late Apop/ early necrosis
Necrosis
5 Gy
MMS
**
NT #4 5 Gy
KIF3A #1 5 Gy
IFT20 #33 5 Gy
IFT88 #13 5 Gy
NT #4 MMS
KIF3A #1 MMS
IFT20 #33 MMS
IFT88 #13 MMS
IR

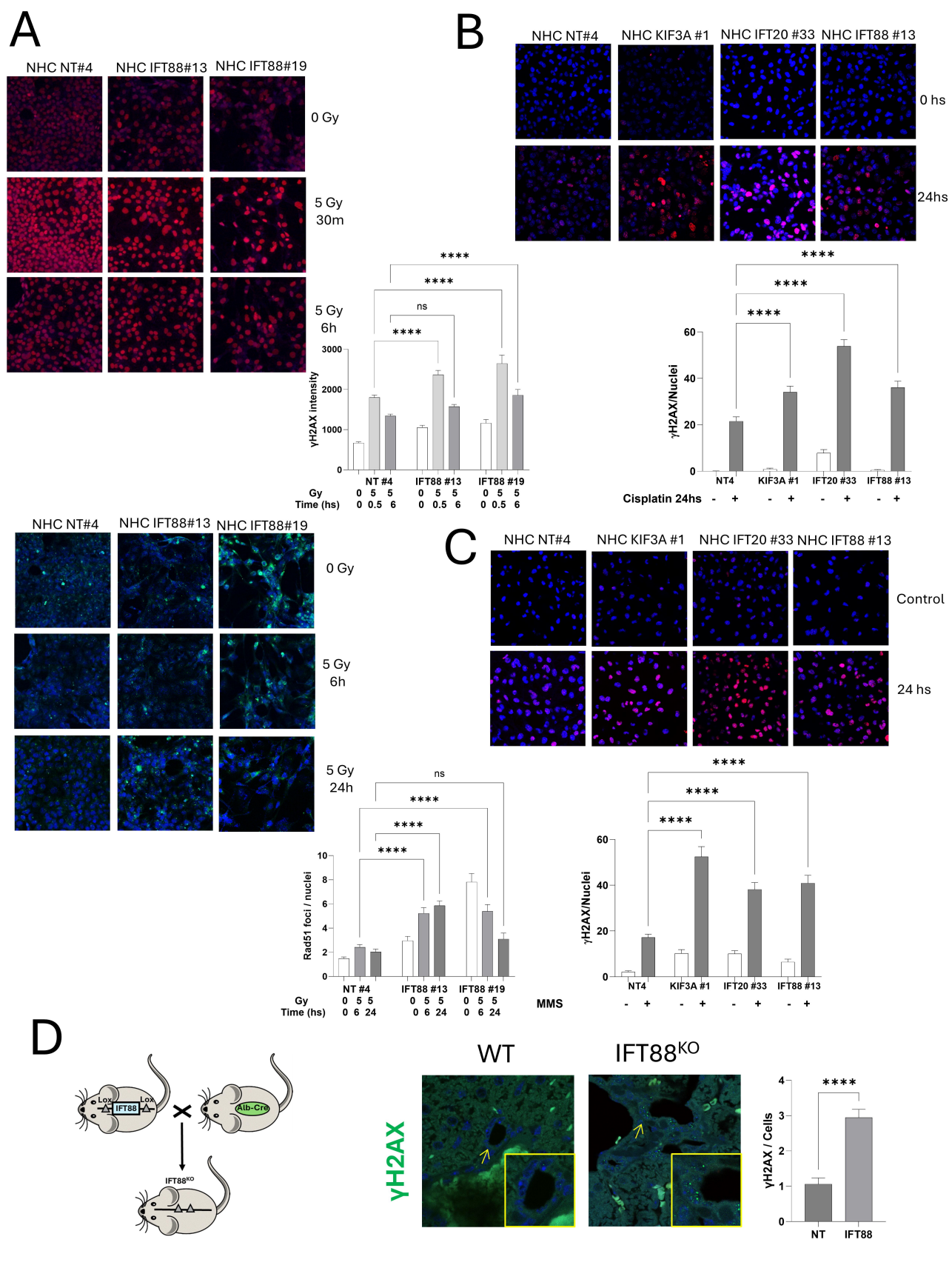
A
NHC NT#4
NHC IFT88#13
NHC IFT88#19
0 Gy
5 Gy 30m
5 Gy 6h
γH2AX intensity
NT #4
IFT88 #13
IFT88 #19
Gy
Time (hs)
B
NHC NT#4
NHC KIF3A #1
NHC IFT20 #33
NHC IFT88 #13
0 hs
24hs
γH2AX/Nuclei
NT4
KIF3A #1
IFT20 #33
IFT88 #13
Cisplatin 24hs
C
NHC NT#4
NHC KIF3A #1
NHC IFT20 #33
NHC IFT88 #13
Control
24 hs
5 Gy 24h
Rad51 foci / nuclei
MMS
D
Lox
IFT88
Alb-Cre
IFT88KO
WT
IFT88KO
γH2AX
γH2AX / Cells
NT
IFT88

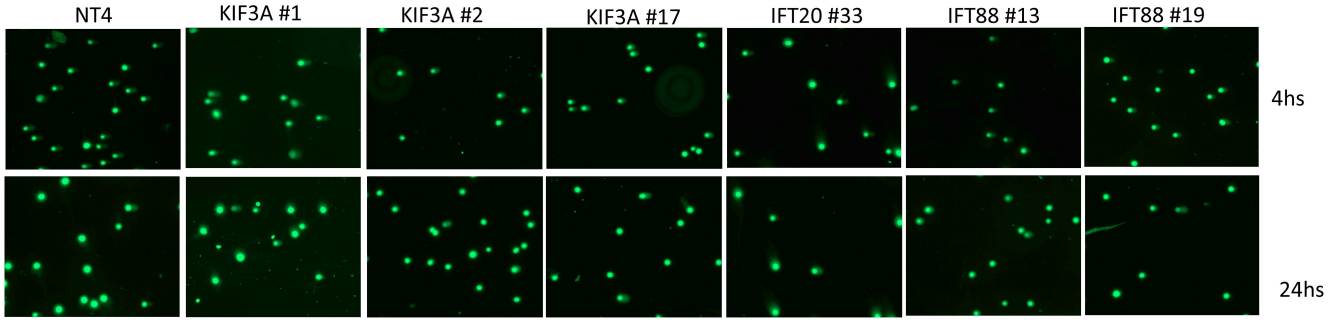
NT4
KIF3A #1
KIF3A #2
KIF3A #17
IFT20 #33
IFT88 #13
IFT88 #19
4hs
24hs

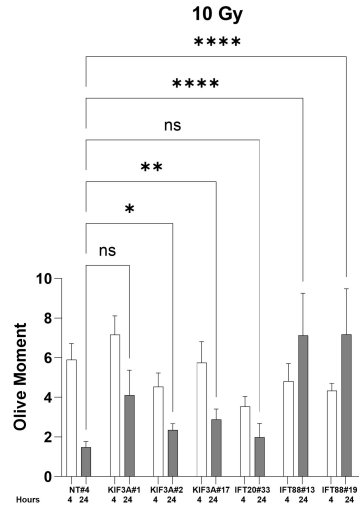
10 Gy
****
****
ns
**
*
ns
Olive Moment
0
2
4
6
8
10
Hours
NT#4 4 24
KIF3A#1 4 24
KIF3A#2 4 24
KIF3A#17 4 24
IFT20#33 4 24
IFT88#13 4 24
IFT88#19 4 24

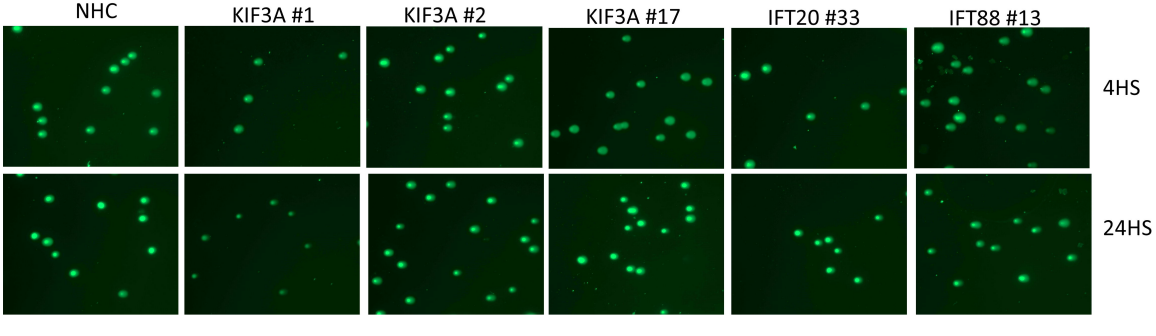
NHC
KIF3A #1
KIF3A #2
KIF3A #17
IFT20 #33
IFT88 #13
4HS
24HS

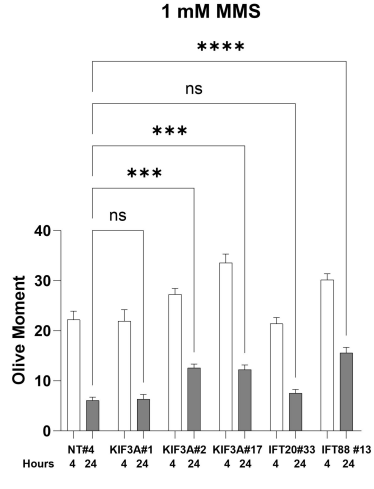
1 mM MMS
****
ns
***
***
ns
Olive Moment
0
10
20
30
40
Hours
NT#4 4 24
KIF3A#1 4 24
KIF3A#2 4 24
KIF3A#17 4 24
IFT20#33 4 24
IFT88 #13 4 24

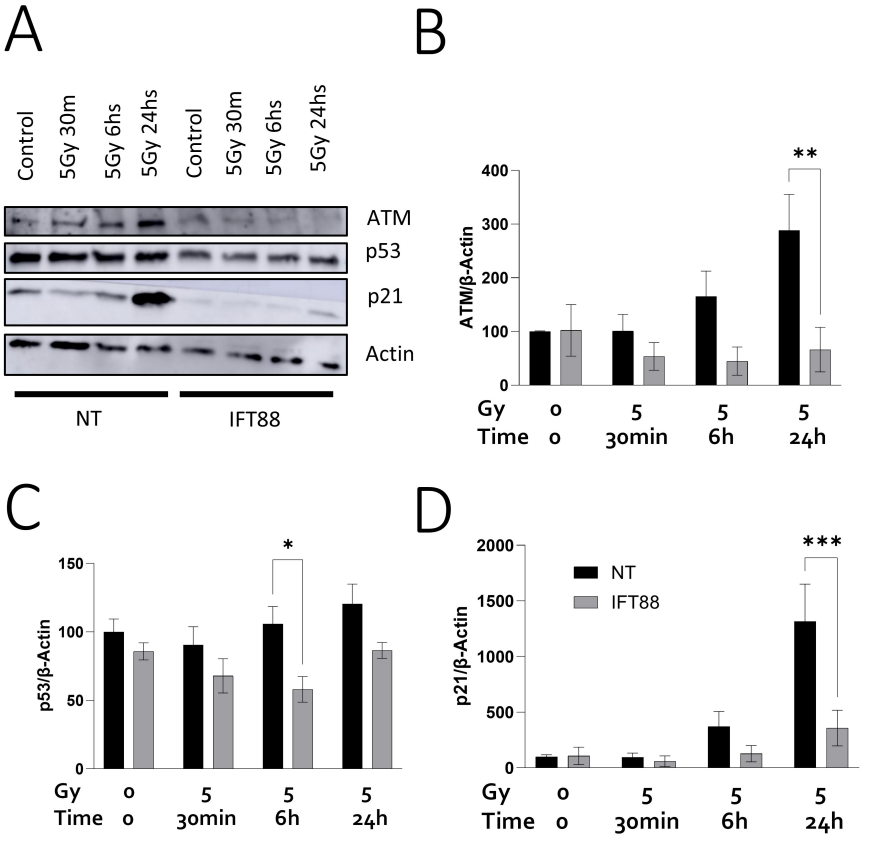
A
Control
5Gy 30m
5Gy 6hs
5Gy 24hs
Control
5Gy 30m
5Gy 6hs
5Gy 24hs
ATM
p53
p21
Actin
NT
IFT88
B
**
400
300
200
100
0
ATM/β-Actin
Gy 0 5 5 5
Time 0 30min 6h 24h
C
*
150
100
50
0
p53/β-Actin
Gy 0 5 5 5
Time 0 30min 6h 24h
D
***
2000
1500
1000
500
0
p21/β-Actin
NT
IFT88
Gy 0 5 5 5
Time 0 30min 6h 24h